Granular Matter (2014) 16:627–640
DOI 10.1007/s10035-014-0516-2

ORIGINAL PAPER

Mechanisms for acoustic emissions generation during granular shearing

Gernot Michlmayr · Dani Or

Received: 12 September 2013 / Published online: 26 June 2014

Abstract Shear deformation of granular media leads to continual restructuring of particle contact network and mechanical interactions. These changes to the mechanical state include jamming of grains, collisions, and frictional slip of particles—all of which present abrupt perturbations of internal forces and release of strain energy. Such energy release events typically result in the generation of elastic waves in the kHz frequency range, termed acoustic emissions (AE). The close association between grain-scale mechanics and AE generation motivated the use of AE as surrogate observations to assess the mechanical state of complex materials and granular flows. The study characterizes AE generation mechanisms stemming from grain-scale mechanical interactions. Basic mechanisms are considered, including frictional slip between particles, and mechanical excitation of particle configurations during force network restructuring events. The intrinsic frequencies and energy content of generated AEs bear the signature of source mechanisms and of structural features of the grain network. Acoustic measurements in simple shear experiments of glass beads reveal distinct characteristics of AE associated with different source mechanisms. These findings offer new capabilities for non-invasive interrogation of micromechancial interactions and linkage to a stochastic model of shear zone mechanics. Certain statistical features of restructuring events and associated energy release during shearing were predicted with a conceptual fiber-bundle model (FBM). In the FBM the collective behavior of a large number of basic mechanical elements (representing e.g. grain contacts), termed fibers, reproduces the reaction of disordered materials to progressive loading. The failure of fibers at an individual threshold force corresponds to slipping of a particle contact or a single rearrangement event of the granular network. The energy release from model fiber breakage is the equivalent to elastic energy from abrupt grain rearrangement events and provides an estimate of the energy available for elastic wave generation. The coupled FBM–AE model was in reasonable agreement with direct shear experiments that were performed on large granular assemblies. The results underline the potential of using AE as a diagnostic tool to study micro-mechanical interactions, shear failure and mobilization in granular material.

Keywords Acoustic emissions · Shear zone formation · Granular mechanics

G. Michlmayr (✉) · D. Or
Department of Environmental Systems Science, ETH Zurich, Zurich, Switzerland
e-mail: gernot.michlmayr@env.ethz.ch

1 Introduction

The link between mechanically-entrained granular media and the generation of sounds has been part of our experiences since we learned to handle rattlers in our early childhood. Such sounds remain familiar in our daily experiences: from the faint trickling of sand in an hourglass to the crunching sounds generated during driving or walking on a gravel road. Deformation-induced sounds are the audible trait of abrupt and episodic grain scale mechanical interactions that release stored strain energy in the form of elastic waves. These mechanical interactions may include collisions of particles, sliding at grain contacts or larger rearrangements within the granular contact network. Different micro-mechanical processes may produce elastic waves with distinguishable frequencies and varying energy content. Perceptible sound is created only when such vibrations are transmitted from solid or liquid surfaces into the surrounding air. A common process that induces abrupt mechanical interactions, associated with elastic wave production, is macroscopic shear

deformation of granular assemblies. The formation of a shear zone is the underpinning mechanism for mobilization of many Earth materials and engineering granulates and can result in landslides, earthquakes, snow avalanches and other rapid mass movements. Elastic waves associated with such processes may deliver valueable information concerning the imminence of large mobilization events.

The inherently non-smooth grain-scale mechanical interactions in grain assemblies lead to several well-known, yet curious phenomena: the localization of deformation in shear bands [1–3], the non-linear properties of wave speed [4–6], or the inhomogeneous distribution of loads in a particle assembly exposed to mechanical stresses [7–10]. Grain-to-grain mechanical interactions are manifested in the behavior of frictional slip, and particle collisions, and the self-organization of a force network.

Such force network typically consists of pillars of aligned and highly stressed grains, so-called force chains [11,12], often oriented along the principal directions of the mean stress field. During progressive shearing, individual force chains undergo repetitive cycles of formation, straining and failure [13]. These cycles are reflected in the intermittent behavior of the sheared granular system . Examples include jamming-unjamming events, stick-slip phenomena or rapid fluctuations of the shear stress [14,15]. For conditions of strain-controlled deformation, granular assemblies typically exhibit fluctuations of stresses [16] (these conditions are contrasted with stress-driven deformation that leads to episodic strain jumps). Similar processes of strain accumulation and sudden release are key to the abrupt occurrence of earthquakes, the triggering of landslides, and the onset of granular flows. The quantitative description of such processes hinges on properly deciphering grain and force network mechanics.

The abrupt rearrangement of a force network, the collision of grains, or friction at particle contacts invariably involve the rapid release of stored elastic energy accumulated during straining. Deformation-induced grain-scale interactions represent various forms of elastic energy dissipation [17,18], ultimately leading to the converting of mechanical energy into heat [19]. Force fluctuations and resulting elastic wave generation (as visualized by Bardenhagen and Brackbill [20] or Owens and Daniels [21]) may therefore offer a means for gauging energy dissipation, and for tracking different pathways of strain energy release. Evidence suggests that the signature of different source mechanisms may be contained in the frequencies and energy of generated elastic waves [22,23].

The deformation of granular assemblies involves a large number of restructuring events at different intensities. Interactions among numerous mechanical elements (grains, force chains), involve large degrees of freedom that are confounded by inherent variability in grain properties and geometrical packing detail. Stochastic methods may overcome the inherent limitations to information concerning geometrical details and individual particle properties in large granular assemblies. A modeling framework for the statistical behavior of systems with many interacting mechanical elements is offered by analogy to fiber bundle models (FBM). The FBM is a conceptual tool capable of representing mechanical interactions and transition processes in disordered materials, such as granular shear zone formation [24,25]. FBMs are based on the interaction of a large number of elements that obey simple mechanical rules and that fail at a stochastically determined threshold strain. Conceptual parallels between elements of the FBM and grain contacts or force chains justify the use of this tool for simulation of complex interactions in granular material. Failure of an element in the fiber bundle would correspond to structural rearrangement in the shear zone eventually, such as buckling of a force chain or particle contact reorganization. FBMs provide predictions of strain energy release associated with those events and can serve to estimate magnitudes of generated AE signals. Hence, FBM-based prediction of AE energies provide a promising starting point to establish links between material mechanics and failure-associated AE generation [24–27]. Analyses of the vibration behavior of prototypical structures provides an inevitable groundwork for the translation of structural rearrangement events into elastic waves. Elastic waves generated during restructuring events radiate from the source location and undergo alterations on their propagation path. If not gauged at the source location (which can hardly be realized in an experiment) such effects may induce considerable bias in inferences based on measured AE events.

The objective of this study was to explore links between grain-scale mechanical interactions in sheared granular materials and associated AE characteristics. We present various mechanisms giving rise to abrupt release of elastic strain energy. We endeavor to investigate how prototypical granular structures release stored strain energy in the form of elastic waves and look at the frequency spectra generated by such energy release events. Here we concentrate on energy release from structural rearrangement events such as repetitive buckling and formation of force chains or micro-slip at single grain contacts. Breakage and comminution of grains as it may occur under excessive loading are not considered. Knowledge of the response of prototypical granular structures to mechanical excitation allows us to bracket typical frequency ranges. The analysis enables a systematic comparison with AE data obtained from shear frame experiments using cohesionless glass bead assemblies. An important practical goal was to establish links between granular material properties, respectively loading procedure and characteristics of generated acoustic emissions. From numerical solutions of the FBM we obtained the statistical description of recurrence of grain rearrangement events and associated AE energies. These results serve to investigate sources of granular material

plasticity and granular material principal mechanical behavior. In this upscaling we also consider contributions of signal attenuation and geometric restrictions of signal acquisition as they occur in real measurement scenarios. The results section compares simulation results with observations obtained from shear tests and measured acoustic event statistics. A concluding section presents consequences of obtained results considering the use of AE from assessment of granular materials. Potentials and limitations of the presented methods will be discussed and further possibilities will be outlined.

2 Modeling grain-scale AE generation

In the following we propose mechanisms for elastic wave generation in deforming granular materials. We first focus on grain-to-grain slip and particle collisions, being mechanisms that occur in prototypical granular material under moderate stresses. The resulting elastic wave frequencies are shaped by the respective source mechanism. In a second step, we provide a mechanistic description of prototypical grain configurations and analyze their characteristics with respect to elastic vibrations. Two different types of events will be discussed: namely elastic waves generated by single grain contact and waves that stem from meso-scale chains of particles. This analysis will enable analyses of simulated structural rearrangement events and their linkage to elastic waves in the forthcoming sections. The analyses of grain-scale mechanical interactions are illustrative and are largely conceptual, nevertheless these theoretical results may sufficiently constrain the expected spectral ranges of resulting elastic waves.

2.1 Particle collisions

During large deformation of granular materials, changes of the grain lattice are inevitable and often involve destruction and reformation of contact networks. The establishment of a new contact by two grains involves a grain collision. The approaching speed of the two grains (and also their geometrical and material properties) determines the energy for the resulting impact. Considering elastic deformation with no shear forces at the contact (standard assumptions of Hertz contact mechanics [28]) the energy involved in the contact deformation is given as:

$$U = \frac{8}{15} E^* R^{*1/2} d^{5/2} \tag{1}$$

where R^* is the harmonic mean of particle radii, E^* the harmonic mean of the Young's moduli (for grains composed of different materials) and d is the indentation depth. The collision of a particle against another particle presents a mechanical impulse imparted on the granular structure. Sufficiently short impulses may be considered as broadband excitation, i.e. equal excitation of all frequencies. For the estimation of the impact duration, t_c, we again invoke Hertz mechanics to obtain [29]:

$$t_c = \frac{4\sqrt{\pi}\,\Gamma\,(2/5)}{5\Gamma\,(9/10)} \left(\frac{m^{*2}}{\frac{16}{15}\,\frac{1-\nu^2}{E^*}\,R\,v} \right) \tag{2}$$

Here $\Gamma\,()$ is the gamma-function, m^* is the harmonic mean of the particle masses, and ν is the material Poisson ratio. Based on Eq. 2 the impact duration for two glass beads ($R = 1 \times 10^{-3}$ m, $m = 11 \times 10^{-6}$ kg, $E = 65 \times 10^9$ Pa, $\nu = 0.23$) during collision at an approach speed of [0.05] m/s is estimated to be 13×10^{-6} s. An impact of this duration may be considered a broadband pulse up to a cut-off frequency of 77×10^6 Hz [30], which is the inverse of the collision time t_c. The non-linear stiffness of a Hertz contact adds to the complexity of modeling forces during particle collisions. Seeking a simple description of the force development, we invoke an approximation made by Hunter [31], that have shown that the process can be described reasonably well by a sinusoidal function.

2.2 Frictional slip

Shear deformation of granular media involves a considerable number of frictional slip events between pairs of grains [32–34]. Studies have shown that dry friction between two rough bodies is a result of the interlocking of surface asperities [35]. Sliding of the two bodies requires deformation or rupture of those asperities. Repetitive sequences of surface interlocking and release during frictional slip constitute dynamic friction force. This apparently constant force consists in fact of microscopic fluctuations around a mean value. Statistical rules for this force fluctuations can be obtained from microscopic features of the surface topography. The self-similarity of surface asperities can be used for deriving frequency-magnitude spectrum of force fluctuations. Along these lines, probabilities of force fluctuations are predicted to decay with $1/f^2$ [36], where f is the recurrence frequency of an event. Following Zaitsev [36], we will use the $1/f^2$-frequency spectrum to describe frictional slip between two grains. Although this frequency characteristic can be assumed to hold only in a certain range (bracketed by the largest and smallest effective asperity) it offers a valid starting point for our considerations. microscopic force fluctuations can be attributed to friction-induced elastic waves [37]. This relation is well established and has been explored already in various studies [18,38–40].

2.3 Single grain excitation

One of the simplest geometrical assemblies built from equally sized spheres is the tetrahedron. This configuration consists of a single particle supported by three neighboring

particles (see inset of Fig. 1), and forms a basic building block of 3-D granular assemblies [41]. Due to its relevance for dense granular media we investigate the response of this structure with respect to mechanical excitation. To obtain the elastic properties of the four-grain configuration, we invoked again the theory of Hertz [28] and find for the stiffness k_{ij} of a sphere-to-sphere contact:

$$k_{ij} = \left(\frac{3F_n R^*}{4}\right)^{1/3} \left(\frac{E^*}{1+\nu^2}\right)^{4/3}. \tag{3}$$

Equation 3 implies that the contact stiffness depends on the contact force F_n, respectively on the compliance induced by this force. In the following, we assume that contact deformation due to static loads is larger than during dynamic oscillations (similar to the assumptions made by Somfai et al. [42]). Correspondingly, we neglect changes of k_{ij} during the resulting particle motion. For the dynamical analysis, viscous damping was considered at the particle contacts. The damping coefficients d_{ij} were set to a small finite number proportional to the corresponding contact stiffness, such that the condition of proportional damping [43] is fulfilled. This additional constraint on d_{ij} allows a relatively simple calculation of a system frequency response function. The starting point for the analysis of particle vibrations is the equation of motion, that relies on the balance between inertial, elastic and viscous forces. For the free particle of our tetrahedron this reads in index notation as

$$m_x \ddot{r_x} = -d_x \dot{r_x} - k_x r_x \tag{4}$$

The effective damping coefficients d_x and effective stiffness k_x are obtained by conversion of the contact quantities (d_{ij} and k_{ij}) from the grain contacts reference frame into global (Cartesian) coordinates. Considering the three spatial coordinates $\{x\ y\ z\}$ Eq. 4 can be expressed equally as three equations. These differential equations are typically solved by assuming a harmonic solution function of the form $\exp(i\,rt)$ [43]. The characteristic frequencies of such oscillation ω_r can also be obtained from an eigenvalue analysis of the equivalent undamped system. Including the effect of damping into the mechanical analysis, a dispersion of the frequency spectra, i.e. response of the system at frequencies other than ω_r can be found. The complete frequency response of the damped system can be expressed as [43]

$$R_x = \frac{1}{k_x}\left(\frac{\left(1-\left(\omega/\omega_{r,x}\right)^2\right) - i\left(2\zeta_x \omega/\omega_{r,x}\right)}{\left(1-\omega/\omega_{r,x}\right)^2 + \left(2\zeta_x \omega/\omega_{r,x}\right)^2}\right). \tag{5}$$

Here $\zeta_x = d_x/2\sqrt{k_x m}$ is the damping ratio at the resonance frequency $\omega_{r,x}$. Equation 5 is derived from the system response function that can be formulated in the Laplace domain. It delivers the resulting amplitude and phase shift when we excited the system with a continuous unit sine of frequency ω. Figure 1a shows resonance frequencies and magnitude of the frequency response $|R_x|$ (including damping) of the active particle in a tetrahedral grain configuration under different confining stresses. Higher static loading results in stiffer contacts and correspondingly higher resonance frequencies ω_r of the structure (note that $\omega_r \sim \sqrt{k/m^*}$). In our example, which was chosen to represent particles in our experimental system, ω_r ranges between 30 and 60 kHz. In addition to the pure frequency response function we considered the system's response to different excitation mechanisms. Idealizing a collision against the free particle (Fig. 1b) as a half-sine-wave, it can be seen, how resonances of the structure are excited. In Fig. 1c we replaced the excitation force with $1/f^2$-fluctuations (duration 130 µs, overlaid with a Hamming window). Again, the resulting vibration is dominated by the resonance of the tetrahedron-structure. However, the excitation mechanism leaves a clear signature in the frequency spectrum, such as the presence of considerable low-frequency contributions in the amplitude spectrum.

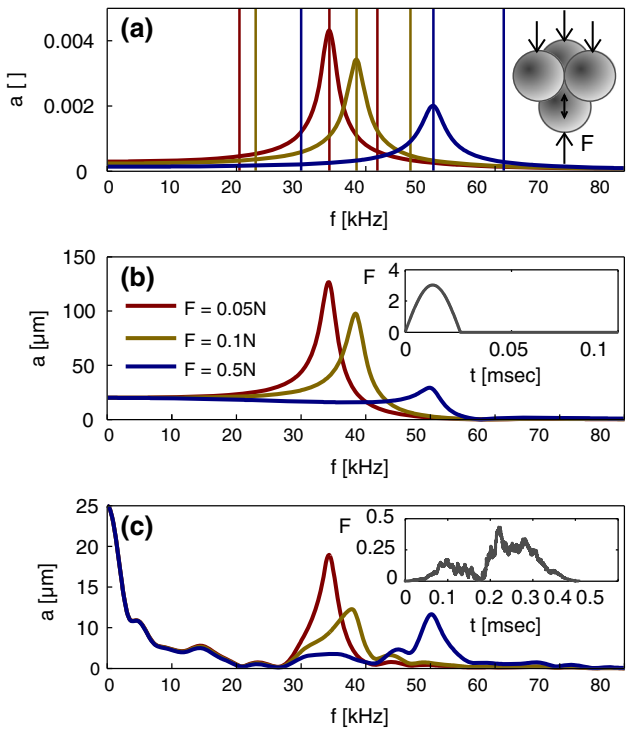

Fig. 1 **a** Frequency response of a tetrahedron-shaped grain assembly (as shown in the *inset*) under different confining loads. Characteristic frequencies are indicated by the *vertical lines*. **b** Response of the tetrahedral structure to excitation from a collision-induced force pulse, as shown in the *inset*. **c** The amplitude spectrum of the calculated response to force fluctuations generated by frictional slip; the time dependent excitation force (in mN) is displayed in the *inset*. (Note that the legend of the center panel applies to all data shown!) (color figure online)

2.4 Excitation of force chains

The mechanical back-bone of granular assemblies subject to shearing is typically formed by force chains. Those are mesoscopic structures of aligned particles bearing an over-proportional large amount of load. The relevance of this structure for granular material mechanics [11,12,44] motivated our dynamical analysis of granular chains in the following.

The derivation of the frequency response is based on mechanical analysis of an idealized force chain as depicted in the inset of Fig. 2. We consider an assembly of spherical masses connected by springs. Analogous to Eq. 4, this simple mechanical model may be expressed as a matrix equation [42]:

$$M\,\ddot{x} = H^T D H\,\dot{x} - H^T K H\,x, \tag{6}$$

The diagonal matrix M represents particle masses and the vector x indicates particle positions. On the right hand side we have the contact stiffness matrix K containing normal and tangential stiffness of all particle contacts. H is called the contact matrix [45] and enables coordinate transformation between the different reference frames (contact reference frame and particle reference frame). Viscous contact damping is included in the equation of motion by the damping matrix D (again we selected the entries of D such that proportional damping is satisfied). Rearranging the terms of Eq. 6 yields:

$$\ddot{x} = -M^{-1} H^T K H\,x - M^{-1} H^T D H\,\dot{x}. \tag{7}$$

Solutions of this system of second order differential equations include harmonic functions that describe oscillatory motions of the particles [42]. Note that the terms $H^T K H$ and $H^T D H$ are symmetric and singular (i.e. not invertible) matrices. M in our case (no consideration of rotational degrees of freedom) has entries only in the main diagonal. Inversion of M under this condition becomes trivial. For the solution of the equation of motion a sufficient number of boundary conditions has to be introduced: here we fix the position of the first and last particle of a granular chain. The eigenvalues and corresponding eigenvectors of the undamped system (represented by the term $M^{-1} H^T K H$) enable derivation of the characteristic oscillation frequencies. The number of characteristic frequencies corresponds to the number of degrees of freedom of the mechanical system, and are indicative of the natural resonance frequencies of the structure. Here we consider only translational degrees of freedom, hence, a chain of N particles will have $3 \times (N-2)$ oscillation frequencies (two particles have fixed positions, so we have to subtract those DOFs). Entries of the stiffness matrix, K (containing bilateral stiffness of all grain contacts), can be determined according to Eq. 3 from grain geometry, material properties and static contact force. Again, we do not consider changes of those entries of K during an oscillation cycle.

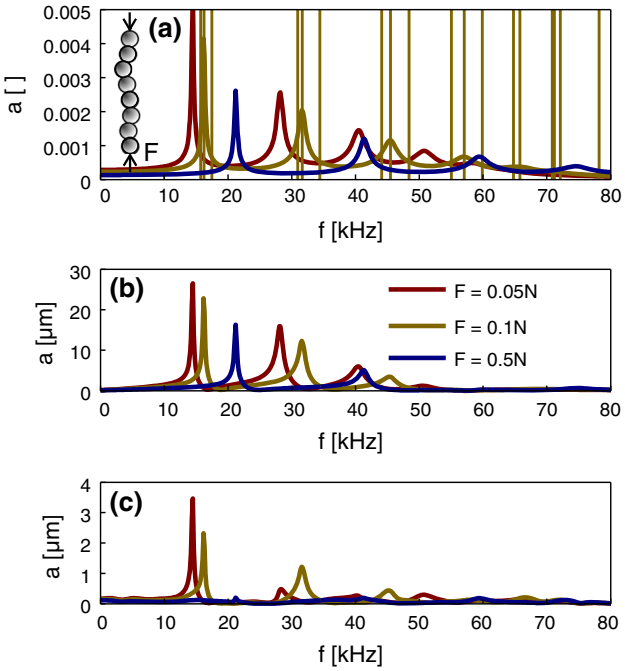

Fig. 2 **a** Excited force chain of 6 free particles (see *inset*) and the resulting frequency response spectra under different normal loads. Eigenfrequencies (in this example we have $6 \times 3 = 18$ distinct resonance modes) of the structure are indicated by *vertical lines*. **b** The frequency response due to particle collision with a force chain. **c** Frequency response after friction excitation. (Note that the legend of the center panel applies to all data shown!) (color figure online)

The model enables a systematic study of the frequencies produced by a particular granular structure. Here we selected a prototypical example of a force chain and computed generated frequencies of an excited particle. Figure 2a shows frequencies of a three-dimensional idealized force chain that consists of eight particles. The figure shows how different normal loads change the characteristic frequencies and their maximum amplitude. It can be seen that oscillations for the considered example have characteristic frequencies greater than 10 kHz. A larger normal load on the force chain yields stiffer contacts and results in higher resonance frequencies. On the other hand, we find higher damping of configurations in the frequency response curve under large normal confinement.

The frequency response in Fig. 2a describes the spectral signature of a grain arrangement. To consider effects of the excitation mechanisms discussed above we modeled the frequency response of the structure to a short force pulse (representing a particle collision) and a succession of $1/f^2$ force fluctuations (representing friction generated vibrations). Figure 2b shows the broadband excitation generated by a particle collision modeled through a 13 µs sine-shaped force pulse. It can be seen that resonance modes above the cut-off frequency (77 kHz) are almost not present in the resulting amplitude

spectrum. Only the lowest resonance frequencies are excited by the collision. Under friction excitation, we also find a cut-off for high resonance frequencies. Since $1/f^2$-fluctuations carry most energy at the low frequencies, it is the lowest resonance frequencies that are responding strongest to this excitation mode.

3 Statistical description of grain scale interactions

3.1 The fiber bundle model (FBM)

The proper integration of individual AE event generation mechanisms, requires an upscaling procedure that establishes direct links to resulting AE activity in granular assemblies. As a first step, we quantify the numbers and intensities of grain-scale restructuring events associated with progressive formation of a shear zone. To bridge the information gap concerning inherent variability of material structure, geometry and properties—all of which crucially determine mechanical behavior—we use a special form of the FBM. FBMs provide a stochastic framework to describe transition phenomena in disordered material [26,46–48]. They consider mechanical interactions among a large number of elements, called fibers. In a their simplest representation such fibers behave as linear-elastic elements breaking at a threshold force that is stochastically determined for each fiber. The standard FBM was developed to describe tensile loading of yarn strings [49,50]. The model was subsequently modified and expanded to consider other loading scenarios, such as bending [51], compression [26] and shearing [47,52]. Building up on a variant of the FBM presented by Halsz and Kun [53] and Halsz [54], Michlmayr et al. [24,25] reproduce key characteristic features of granular shearing and associated acoustic signals. In the annealed disorder FBM, by Michlmayr et al. [24], broken elements are replaced by new, unstrained fibers that receive a new random rupture threshold. Fibers in this annealed disorder FBM undergo series of rupture and reconstitution cycles, reminiscent of continual force chain reformation or repetitive frictional slip between grains. Different statistical distribution functions may be used for the assignment of fiber threshold values t. The two parameter (m and λ) Weibull distribution function appears particularly useful for this task, because of its simplicity and the inherent link to failure processes:

$$p_t(t) = \frac{m}{\lambda}\left(\frac{t}{\lambda}\right)^{m-1} \mathrm{e}^{-(t/\lambda)^m} \tag{8}$$

Earlier work provides us with detailed analysis of the annealed FBM mechanical behavior and energy release associated with fiber rupture [24,25,53,54]. Here we consider annealed fiber bundles consisting of N elements, representing active particle contacts of a granular shear zone. The fiber elements in our model are arranged on a square lattice. The spatial arrangement of fibers does not affect the mechanical behavior of the bundle, however, for later considerations of attenuation the location of element failure becomes a crucial factor. The stress strain behavior of the bundle naturally depends on the failure-restoration history of its fibers. It can be written in rate form as

$$\frac{\Delta\tau}{\Delta\varepsilon} = NE\Delta\varepsilon - \sum^{N_f} t_i \tag{9}$$

where E is the fiber elasticity and N_f indicates the number of breaking fibers within the strain interval $\Delta\varepsilon$. The constitutive behavior of this system is a result of the competition between elastic deformation of elements during a strain increment (represented by the first term of the right-hand-side of Eq. 9) and element failure during a strain increment (as described by the summation term in Eq. 9). The first contributes to an increase of the total shear force while the latter facilitates abrupt decays of the resulting forces. A more detailed description of the mechanical behavior of such annealed disorder fiber bundles can be found in our earlier work [24,25]. The energy that is released during fiber rupture events can be expressed (also in rate form) as

$$\frac{\Delta U}{\Delta\varepsilon} = \frac{1}{E}\sum^{Nf}\frac{t_i^2}{2} \tag{10}$$

Considering elements of the FBM as conceptual representation of grain contacts and force chains, the expression above represents the energy released during granular restructuring events and associated AE generation. As presented in the previous section, AE may be generated by different mechanisms during granular shearing. Those mechanisms may affect either single grains or an entire group of grains. Because the magnitude of such restructuring events appears as the main control to govern the level of grain excitation we group fiber rupture events according to their rupture threshold. This is based on the perception that failing elements in the strong force network will excite the remaining network. The effect of weak element failure is assumed to only lead to vibration on the single grain scale. The fraction of particles that form this so-called "strong" force network is a matter of ongoing discussion and based on the definition criteria estimations range from 20 % [12] to less than 10 % [55]. Based on this values we consider the strongest 10 % fibers ($0.9\,t_{max} < t \leq t_{max}$) to constitute the "strong" force network potentially exciting force chains during a reorganization event. The remaining 90 % fibers ($0.9\,t_{max} < t \leq t_{max}$) will be assumed to belong to the "weak" network that will induce single grain vibration at failure (in both cases t_{max} indicates the maximum fiber strength value at a given bundle deformation).

The two primary theoretical quantities of interest, namely the fiber bundle stress τ and the energy release rate $\Delta U/\Delta\varepsilon$ can be directly compared with measurements of force and AE obtained during shearing of real granular systems. Since both measures can be expressed only in a rate form, we performed step-wise calculation of the bundle behavior according to the following procedure:

1. attribute initial rupture thresholds to all N fibers,
2. increase the strain up to the threshold t_i^k of the weakest fiber of the bundle,
3. after rupture a fiber receives a new random threshold t_i^{k+1}, the straining of the fiber is reset to zero, the next failure of this fiber will take place at $\sum_{q=1}^{k+1} t_i^q$.
4. repeat 2 and 3 to continue straining of the fiber bundle.

Previous studies [25] have shown that an annealed disorder FBM can reproduce complex granular shear zone formation considerably well: Fig. 3 shows the shear stress τ on a fiber-bundle consisting of $N = 10^5$ elements; thresholds t are drawn from a Weibull distribution with $m = 2$ and $\lambda = 1$ (parameter selection is based on failure rate of granular contacts and has yielded good agreement of the model with observations [25]). Similar to the results presented in earlier work [25] we find stress-features characteristic for granular materials under shear deformation: that is the build-up of shear stress with increasing plasticity at the onset of shearing (phase a–b in Fig. 3), followed by the peak shear stress and relaxation into a residual stress regime (phase b–d in Fig. 3). Simulations of the energy release rate $\Delta U/\Delta\varepsilon$ are in agreement with analytic results presented earlier [25]. The results show a delayed increase in energy release rate relative to the increase in shear stress. The metrics of energy release exhibits larger fluctuations than the bundle stress that reflects the state of intact fibers. The inset of Fig. 3 shows the statistics of energy release rates U (this is the energy released from a single fiber at its rupture threshold t, hence $U = E\,t^2/2$) at different phases throughout the straining process. A comparison of both empirical distributions shows how an increasing amount of large events shapes the energy release as deformation advances.

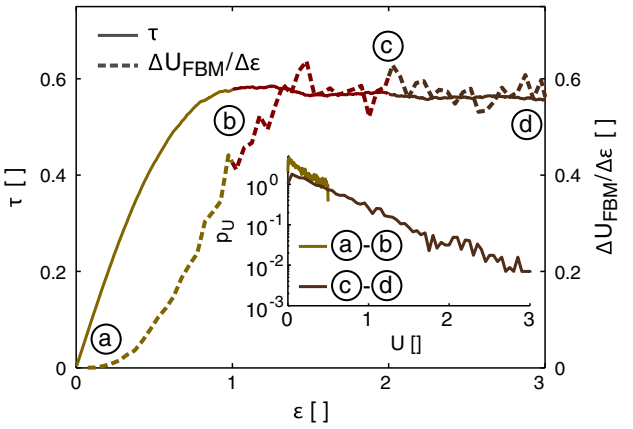

Fig. 3 Stress strain curve of the annealed disorder FBM consisting of $N = 10^5$ fibers. The *insets* show statistics of rupture associated energy release (U) at the beginning (a, b) and at the end (c, d) of the straining process (color figure online)

3.2 Attenuation of AE signals, a sensor's field-of-view

Elastic waves undergo considerable damping and wave distortion while propagation through granular media. To model attenuation of elastic waves as they travel from the source location to the sensor we employed a simplistic geometrical decay model. We neglect any other attenuation mechanisms, and consider the total elastic energy in a wavefront E to remain conserved while it radiates from the source location r. The spherical divergence of the wave with distance from the source is associated with decay of the energy density E_0 according to:

$$E_0 4\pi r_0^2 = E 4\pi r^2 \tag{11}$$

$$E = \left(\frac{r_0}{r}\right)^2 E_0. \tag{12}$$

Here we assume that the elastic energy is concentrated at the propagating wave front that has the shape of an expanding spherical shell. Depending on the propagation distance, the original amount of emitted energy E_0 decays with the distance from the source as r^{-2}. Signals generated away from the sensor are more attenuated and appear weaker (low amplitude). This simple geometric damping was included in into our conceptual shear zone model as shown in Fig. 4. We assume that elastic wave generation takes place at a plane Σ only. Σ represents the shear zone. A sensor is located at a distance r_0 facing this plane. The previously described FBM delivers rate and energies of element failure events. The square lattice arrangement of the fibers allows to attribute a spatial coordinate on the plane Σ to each of those failure events.Using the fiber position the distance to a stationary virtual sensor be derived and consequently the relative geometric damping (as compared to a similar event at distance r_0).

Figure 5 shows the effect of the above described mechanisms on a FBM-generated distribution of energies generated within a plane. The FBM used in this simulation consists of 19,600 elements. The figure shows empirical distributions of event energies at the source (undamped events) and at the sensor (damped events). We distinguished between different source mechanisms in our mode according to the fiber failure threshold: strong fibers stood for force chain excitation and weak fibers represented grain excitation (as described in the previous section). Comparing statistics of signal energies at their source (no damping) with the frequency-magnitude

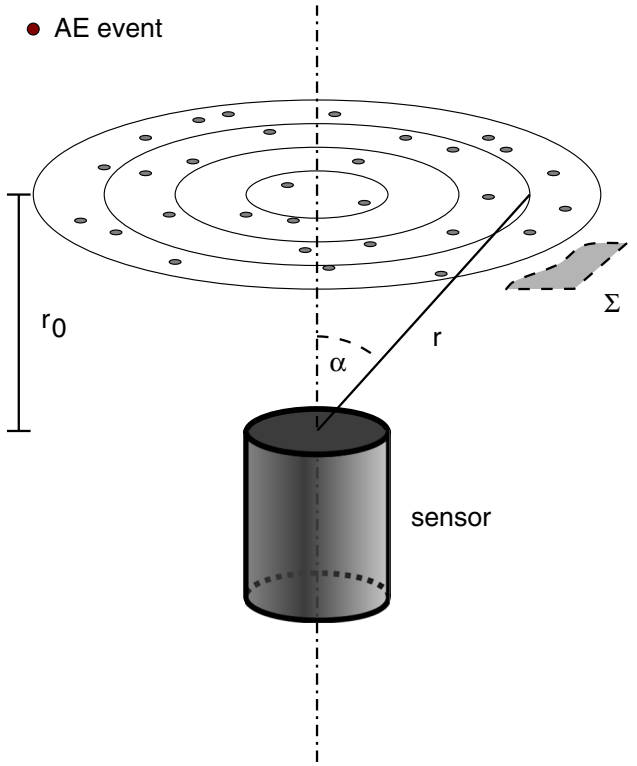

Fig. 4 Cone of detection intersected with the shear plane Σ yields the region of detectable AE events. The distance between sensor and shear plane r_0 determines together with the signal incident angle α the propagation distance r between a signal source and the sensor

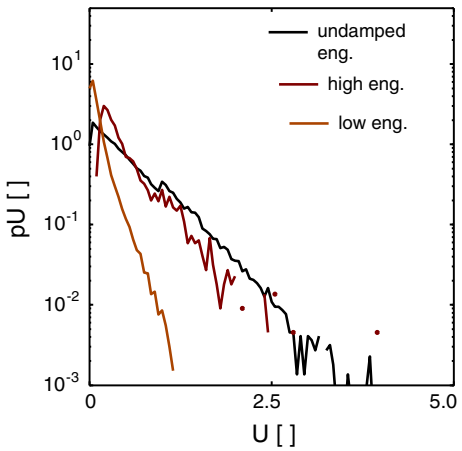

Fig. 5 Change of the event frequency-magnitude distribution by the proposed propagation model for three fiber bundles of different sizes: **a** $N = 19{,}600$, and **b** $N = 1{,}225$. *Gray lines* indicate empirical probabilities of original (undamped) signals. *Colored lines* give distributions of damped signals from weak and strong fibers. (Note that the legend of the left panel applies to all data shown!) (color figure online)

distribution of signals at the sensor we find clear differences that reflect the effect of damping. Signals generated from failure of weak fibers show a strong deviation from the original distribution after undergoing damping. Failure of strong fibers is associated with high energy events, which are less affected by signal damping. The distribution of damped signals remains almost entirely conserved compared to the original frequency-magnitude distribution with only a truncation at the right end (where the highest energies reside).

4 Experiments

4.1 Shear frame setup

Shear deformation of large granular assemblies were measured using a linear shear frame apparatus (previously described in Michlmayr et al. [25]). The sample container consisted of two frames with dimensions of 0.15 m × 0.15 m × 0.15 m. The lower frame is supported by linear roller bearings to allow horizontal motion in one direction. Displacement is applied by a linear driver (*PERO* linear spindle motor, PERO GmbH, Germany) pulling the lower frame at a constant rate. A normal load was applied to the sheared granular sample using a pneumatic cylinder. The experimental setup is shown in the sketch of Fig. 6 and is similar to the direct shear test used in for geotechnical testing [56]. A numerical analysis of this setup was provided by several authors [57–60]. It shows from those publications that shear deformation typically localizes in a narrow lenticular shear zone. The width of this shear zone is often assumed to be 10 times the average grain size (e.g. based on the numerical experiments by Liu [59]). Force sensors attached to the upper frame allowed to measure shear forces during the displacement procedure. Forces were recorded at high temporal resolution ($1{,}620\,\mathrm{s}^{-1}$) allowing to resolve rapid stress fluctuations with magnitudes >30 Pa. For measurements of elastic waves, two types of acoustic transducers were placed within the sample material during the shear tests. A 1-D accelerometer (*MS ACH-01, Measurement Specialities Inc., USA)* with a sensitivity of $0.92 \times 10^{-3}\,\mathrm{V\,m\,s^{-2}}$ and a linear frequency response in the range <20 kHz was placed in the upper frame 0.05 m above the imposed shear zone in a way that it could captured elastic waves normal to the shear plane. Additionally, we captured high-frequency acoustic emissions in the range of 30–80 kHz using piezoelectric sensors (VS75-V, by Vallen, Germany, for frequency response see inset of Fig. 8). All sensors were placed close to the shear plane embedded within the granular material. To extract discrete events from the continuous waveform captured by the different sensors a constant threshold was applied. Signals that exceed this threshold are assumed to be associated with mechanical failure events within the material. Digitalized signals are provided in units of voltage. Note, that frequency-dependence of the sensor response, pre-amplification, and A/D-conversion makes the recovery of original signal shapes a non-trivial task. In this work

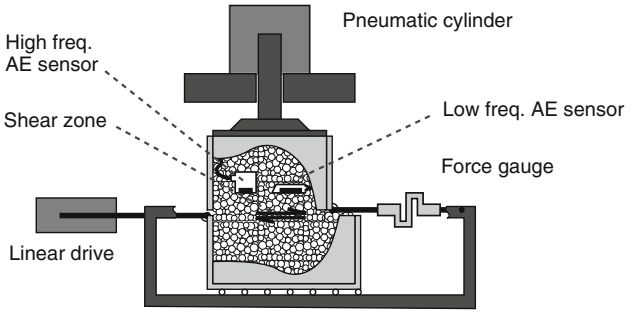

Fig. 6 Sketch of the shear test setup. The frames containing the granular material are cut open for better visibility of sensor positions. Normal load is applied with a pneumatic cylinder. A linear motor allows to maintain deformation at a constant speed

we instead provide signal amplitudes from the digital wave form only and derived energy measures from time integration of signal voltage respectively as non-physical energy units.

We have used different types of spherical, narrow-graded soda-lime glass beads (SiLi beads type S, Sigmund Lindner GmbH, Germany) for performing granular shear tests. The glass density was 2.5 kg m^{-3} and the Young's modulus 63 × 10^9 Pa. Tests were performed using two different grain sizes: 3.8–4.4 and 1.0–1.3 mm.

For comparison with model predictions we estimated the number of particles in the shear layer as 1,225, and 19,600 respectively. In all tests reported here, the granular sample was air dry. The glass beads were filled into the shear frame in three layers, that were compacted each by tapping with a hammer. Acoustic sensors were placed within the sample material during this procedure. After leveling the sample material at the surface it was covered with a 2 mm-thick rubber pad to provided a homogeneous distribution of applied normal loads. Tests were conducted at different normal stresses: 30, 45, and 60 kPa. The displacement rate during experiments was maintained constant at 0.033 mm s^{-1}.

Data streams were synchronized before further analysis. Frequency spectra from low-frequency acoustic emission events were obtained by Fast-Fourier transformation. To avoid aliasing-effects in frequency spectra a Hamming window was applied to the data frames (each data frame contained one AE event).

4.2 Experiment results

4.2.1 Examples of signal waveforms

The formation of a shear zone in granular materials and associated micro-mechanical restructuring events manifest in development of shear stresses and simultaneous generation of AE signals. Links between the mechanical and acoustic facet of shearing can be illustrated with the example of a direct shear test shown in Fig. 7. We found that under the given test conditions, the measured shear stresses exhibited considerable fluctuations around an average value. A consistent link between such stress jumps and the release of low-frequency AE signals has been shown already in a previous study [25].

These fluctuations show different characteristics during (1) a jamming phase where shear stress builds up constantly, (2) a plastic phase, that features decaying stress accumulation including smaller stress tremor and release events, and (3) a full stress release events, characterized by an abrupt and considerable jump of measured shear stress. Visual inspection of the results indicates that the measured stress jumps and acquired low frequency AE signals were highly correlated in their occurrence times. In some cases, a stress tremor and precursory jumps during plastic material deformation triggered smaller low-frequency AE events. The three last force jumps in the expanded example in Fig. 7 show such tremor-induced low-frequency AE events during the plastic phase.

High-frequency AE measurements (Fig. 7c) in our example delivered more events than their low-frequency counterparts. An strong connection to stress jumps can not be deduced immediately from this sample data set, since signals were captured during all three phases of a stress jump cycle. However, the presented example suggests an increase of AE intensity (i.e. rate and magnitudes) at the imminence of a stress jump. Immediately following a stress release event,

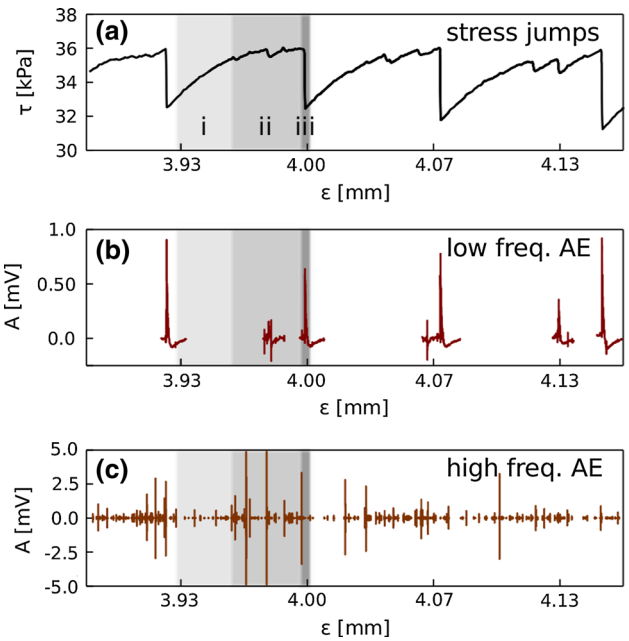

Fig. 7 **a** Stress jumps during a shear experiment with 4 mm glass beads under a confining stress of 60 kPa with concurrent record of **b** low-frequency AE signals and **c** high-frequency AE events. Different phases of a characteristic stress jump cycle are illustrated for a single restructuring event marked by *gray boxes* (color figure online)

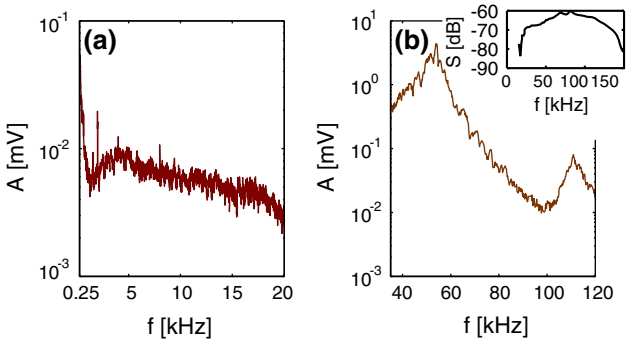

Fig. 8 **a** Measured average frequency spectra captured by the low frequency AE system (acceleration amplitude spectrum) and by **b** the high frequency AE system (pressure amplitude spectrum). The inset of panel **b** shows the characteristic response function of the high frequency sensor within the frequency range of interest expressed in dB re 1 mV/bar (color figure online)

the generation of high-frequency AE events remained quiescent for a short period of time.

4.2.2 Typical frequency ranges of observed AEs

Mechanical considerations for quantifying AE events generated by grain-scale interactions were presented in Sect. 2. To experimentally evaluated predicted frequency ranges we analyzed signals collected during direct shear tests of glass beads. The transformation of AE signals into the frequency domain using standard Fourier transformation allowed comparison of measurements with modeling results. Measured spectral amplitudes were averaged over many AE data sets to minimize effects of spurious events. Figure 8 shows the average spectra of 29 low-frequency events. The right panel of Fig. 8 displays the average spectrum of 29 high-frequency measurements collected concurrently. All signals were observed during the latter phase of shearing experiments with 1 mm glass beads and a confining load of 45 kPa. We found a general decay of the spectral amplitude for high frequencies in both spectra. This general trend is interrupted by a number of local peaks: at 5 kHz for the low-frequency spectrum, and at 54 and 111 kHz in the spectrum of high-frequency measurements. To rule out a bias from the sensor's own resonance frequencies we provide the sensor frequency-response functions in the inset of Fig. 8. The response spectrum of the AE sensor type (see the inset in Fig. 8) did not exhibit any resonance frequencies at the observed frequency peaks, which suggests that those features represented properties of the material and the AE generation mechanisms. Low frequency AE signals are captured with a broadband accelerometer operating below the first resonance frequency. The response of this sensor can therefore be assumed flat and no interference with the signal spectrum is expected (we therefore do not display the sensor response spectrum in Fig. 8a).

4.2.3 Features of AE response to stress jumps

The illustrative data in Fig. 7 suggests that stress jumps are associated with the two types of measured AE signals we measured in direct shear tests. To improve our understanding of these observations we compared the average AE activity of both sensor types at the imminence of stress release events (see Fig. 9). For the analysis we performed coherent averaging over the stress jumps of a single shear test and associated records of AE events. This process involves collection of multiple consecutive stress jump cycles that originally occurred sequentially in time, and averaging over the force and AE signals for each jump (stacking the sequences with a common origin). This analysis delivered us the mechanical (Fig. 9a) and acoustic (Fig. 9b, c) signature of the "mean" stress jump at different experimental conditions. We observed clear differences between the magnitude of stress jumps amongst tests with different materials. We found that tests with 4 mm grains produced the considerable stronger stress jumps compared to tests with 1 mm grains. For all cases considered, the averaging procedure produced a smooth force curve prior to the release event contrasting precursory stress tremor that has been observed during phase (2) of the previously presented data example (see Fig. 7a). The absence of precursory fluctuations after averaging of signals reflects the random nature of this phenomenon. The corresponding activity of low-frequency AE confirmed a strong link of those signals to stress jumps as it was pointed out already in Sect. 4.2.1: the analysis showed that almost every low-frequency event was observed together (at a displacement difference of less than 0.005 mm) with a stress release event, irrespective of experimental conditions. The results of Fig. 9c show the average high-frequency AE activity in relation to stress release events. From our earlier analyses (see Fig. 7c) we found that those signals occurred during stress accumulation and not only during stress-release events. This was confirmed by Fig. 9c. Also, we were able to reveal a significant increase of high-frequency AE activity at the imminence of stress jumps. Particularly in materials with smaller grains significant high-frequency AE activity was observed prior to stress jumps.

4.3 Modeling AE statistics utilizing the FBM–AE model

The results in the previous sections lend support to the assumption that different micro-mechanical interactions within a granular shear zone produce distinct AE signals. For example, we attribute large rearrangements of the granular lattice to the rupture of force chains. In our experiments such events appeared as fluctuations in the macroscopic shear stress and triggered distinct low-frequency AE signals. Smaller failure events eventually at the level of single grains could be detected by the high-frequency AE events.

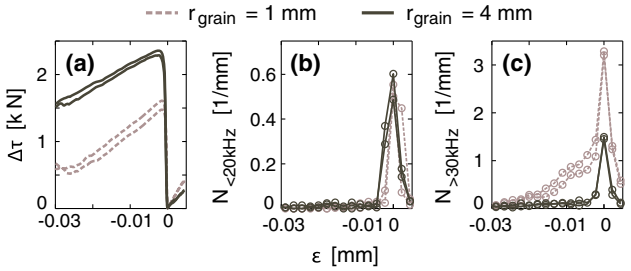

Fig. 9 **a** Coherent averaging over individual stress release cycles under different test conditions ("mean" stress jump). **b** Concurrent low-frequency (accelerometer) AE, and **c** high-frequency AE activity. The normal load in all experiments was 45 kPa

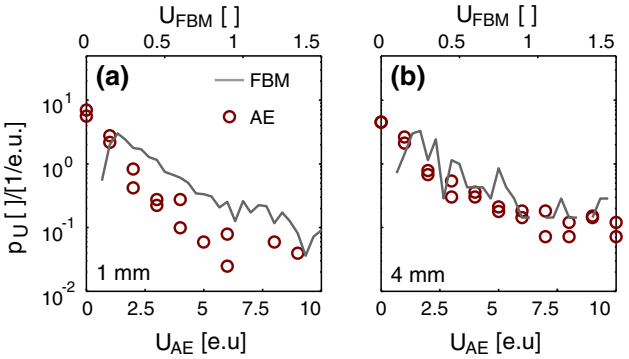

Fig. 10 Size distribution of strong fiber rupture events as generated by the signal-attenuation FBM: **a** comparison between results from a large bundle with corresponding low-frequency AE events from 1 mm grain assemblies. **b** A small bundle represents a physical system with large (4 mm) grains. Again low-frequency AE energies are compared against energies from strong fiber rupture. A proxy for AE energy is obtained from time integral of recorded signal amplitudes and has units of V s (we are aware that in a physical sense this is no energy measure and refer to it as "energy unit") (color figure online)

These however, did not leave a visible signature on the global stress picture in our experimental setup.

For integration into the FBM we attribute low-frequency AE signals (presumably associated to force chain buckling) with the rupture of the strongest fibers in a bundle. High-frequency acoustic events are triggered by smaller and secondary perturbations of the granular force lattice and are consequently represented by the breaking of weak fibers. As described earlier we have set the discrimination threshold between "weak" and "strong" fiber excitation to a value of 0.9 t_{max} (i.e. 90 % of the currently largest failure threshold within a bundle). For comparison with experimental observations we included attenuation of the released energy, as described above (Sect. 3.2). A comparison of attenuated strong fiber energies with low-frequency AE energies is presented in Fig. 10. A reasonable qualitative agreement between observations and model predictions could be found. Difficulties to recover physical units from digitized signals, as mentioned in Sect. 4.1, led us to express AE event energies in terms of arbitrary (non physical) energy units. This surrogate measure of elastic energy release was obtained by integrating the sensor's signal amplitude (voltage) over the duration of the event (units of [V s]). A quantitative comparison with FBM energies is therefore not possible. Nevertheless the coherence of the results between the two test cases in Fig. 10 supports our confidence in the capabilities of the coupled signal attenuation-FBM.

4.4 Modeling force chain restructuring

By separation of fiber-bundle elements into two major fiber types, namely strong ($0.9\, t_{max} < t \leq t_{max}$) and weak fibers ($0 < t \leq 0.9\, t_{max}$), we were able to describe the two primary granular failure mechanisms. Here, rearrangement of strong fibers was associated with stress jump-induced low-frequency AE events; weak fiber failure in the FBM represented minor restructuring events associated with high-frequency AE. For testing model predictions of those different failure types we compared modeled and measured energy release rates. The energy release rate is a measure of the failure-associated energy that is released during a strain increment.

Modeled predictions of total energy release were categorized based on the type of failed fibers as seen in Fig. 11a. The results suggest that energy release rates from failure of weak fibers is characteristically different that energy release from strong fibers. Weak fibers release most of the stored strain energy at the early stage of deformation whereas at latter stages of shear deformation most of the elastic energy release comes from the resilient strong fibers. These model predictions were compared with AE measurements reported in earlier studies [24,25]. The results in Fig. 11b show a reasonable agreement with the characteristics predicted by the FBM model. The delayed onset of energy release from strong fibers can also be found in the energy trace of low-frequency AE signals.

5 Discussion and conclusions

Elastic waves generated during shearing of granular materials contain rich information related to grain scale rearrangements and failure precursors. To obtain a better understanding how material properties, and different triggering mechanisms shape resulting acoustic signals we studied prototypical cases of grain scale-induced elastic wave generation. We focused primarily on grain collisions and particle-to-particle friction as triggering mechanisms of acoustic signals. Based on mechanical considerations we propose a distinct acoustic signature of both processes. Together with the particular triggering mechanisms we assumed that the resonance frequen-

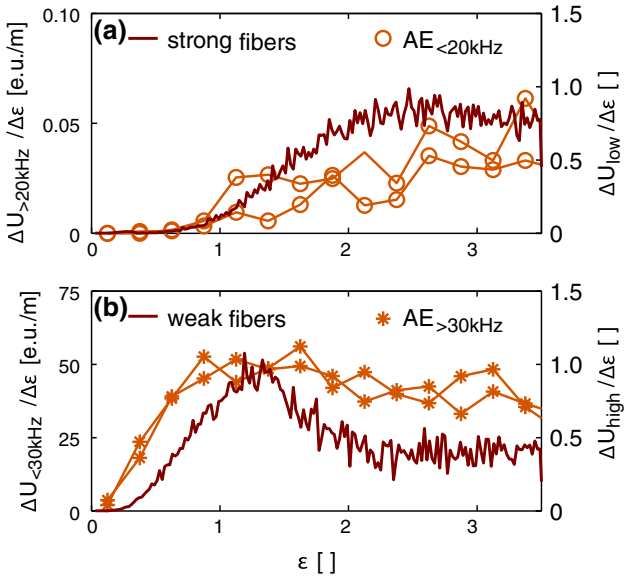

Fig. 11 Energy release rate from different groups of fibers compared against observed data from different AE sensors during shear tests (1 mm glass beads and 45 kPa normal load). **a** Strong fibers ($0.9\,t_{max} < t \leq t_{max}$) are compared against low-frequency AE events ($AE_{>20\,kPa}$). **b** Weak fibers ($0 < t \leq 0.9\,t_{max}$) are shown on the same panel as high-frequency AE ($AE_{<30\,kPa}$) (color figure online)

cies of excited granular structures determine the spectral characteristics of elastic waves. We investigated the effect of those excitation mechanisms on different granular structures. Here we consider excitation of single particles in a tetrahedral compound and of confined granular chains—so-called force chains. Such force chains are known to constitute the primary load bearing structure and to dominate the mechanics of granular shear bands. We invoked eigenvalue analysis of the mentioned prototypical granular structures to localize typical resonances in a frequency range of 10^4–10^5 Hz. The AE source mechanisms were analyzed for idealized configurations and remain primary conceptual (ignoring details of structure and material properties). However, predictions from our model were in good agreement with frequency ranges of AE events observed during granular shearing of glass bead assemblies. Analyses revealed the presence of distinct peaks in the frequency spectra of experimental results that were in the range of predicted resonances.

To model quantitative features and statistics of restructuring events that occur during granular shear deformation we used a fiber-bundle model. In this conceptual shear zone representation material behavior is constituted by a large number of individual elements, termed fibers, that fail independently at a statistically determined rupture threshold. This relatively simple model provides us with predictions of failure statistics and the material stress–strain behavior. Earlier work showed that this FBM can reproduce key features of granular shearing and presented analytical solutions of the model [24,25]. Here we used the FBM to resolve two different restructuring mechanisms that are considered most important in dry prototypical granular materials. For both mechanisms our model allows to track the energetic trace throughout the deformation process: failure of the strongest fibers in the bundle was associated with force chain excitation; rupture of weak fibers was assumed to stand for excitation of smaller structures. Although the formation of a dual force network in granular material is confirmed by a large body of literature, a threshold to distinguish between "weak" and "strong" contacts is difficult to define. Consequently the separation threshold of fibers in our model is rather based on estimates that can be found in the literature than on physical principles, which leaves room for improvement. The agreement with observations as shown in Fig. 11, however, lends credence to this approach. Also we introduced a simple propagation model that relies on the geometric attenuation of an elastic wave. Comparison of modeled failure magnitude distributions with statistics of low-frequency AE events shows a good agreement and legitimates our model.

An important advantage of the FBM lies in the simplicity to predict failure associated energy release. Energy loss from fiber rupture can be related directly to acoustic emissions, heat release, or other forms of energy dissipation. Here we attributed AE generation mechanisms to different rupture events. By comparison with AE data we could show that the FBM predicts characteristic energy release from high-frequency and low-frequency AE events (representing large and small rearrangement events respectively).

Measurable acoustic emissions at different frequency bands were found to be closely related to episodic and abrupt stress release events observed during granular shearing. We were able to demonstrate a direct link between low-frequency AE events and distinct stress fluctuations, presumably expressing large rearrangements of the granular lattice and associated force chain excitation. High-frequency AE activity increased before such rearrangement events typically announcing observed stress jumps. The trace of individual high-frequency events could not be found in the shear stress data. Grain rearrangement events that emit such high-frequency AE signals are presumably too small to induce measurable changes of the total shear stresses in our experimental setup.

6 Summary

The study develops a novel quantitative framework linking grain-scale mechanical interactions with release of stored strain energy in the form of elastic waves. The mechanistic links enable interpretation of measurable acoustic emissions (AE) and establish relations to typically unobservable internal mechanical interactions during shearing of granular

assemblies. We presented dynamic analysis of AE producing processes including derivation of frequency spectra and released energies. Results suggest typical frequencies in the range of 10^4 Hz. The generation process (we have looked at grain-to-grain friction and particle collisions) and the size and geometry of an excited structure leave their signature on generated frequency spectra. For the upscaling of this micromechanical analysis to the scale of an entire shear plane, we used a conceptual fiber-bundle model. Effects of signal attenuation were considered with a geometric damping model. We were able to show that signal damping leaves a strong footprint in the way a single sensor captures distributed signals from ongoing granular shearing. Particularly low magnitude AE source events—we associated those with the "weak" elements in our model—are affected by damping. So-called "strong" elements in the FBM were related to force chains. They have the propensity to withstand the material deformation longer and to release more energy upon failure. Results of our model were compared against measurements from shear frame tests. Evidence suggests that instantaneous observations of low (<20 kHz) and high (>30 kHz) AE events provide complementary information concerning formation of shear zone and stress release events.

Acknowledgments This study is part of "Triggering of Rapid Mass Movements" (TRAMM) funded by the Competence Center Environment and Sustainability (CCES) of the ETH domain (Switzerland). The authors wish to thank Daniel Breitenstein for his technical support with the experimental work presented in this paper.

References

1. Vardoulakis, I.: Shear band inclination and shear modulus of sand in biaxial tests. Int. J. Numer. Anal. Methods **4**(2), 103–119 (1980)
2. Oda, M., Kazama, H.: Microstructure of shear bands and its relation to the mechanisms of dilatancy and failure of dense granular soils. Geotechnique **48**(4), 465–481 (1998)
3. Desrues, J., Viggiani, G.: Strain localization in sand: an overview of the experimental results obtained in grenoble using stereophotogrammetry. Int. J. Numer. Anal. Methods **28**(4), 279–321 (2004)
4. Liu, Ch., Nagel, S.R.: Sound in sand. Phys. Rev. Lett. **68**(15), 2301–2304 (1992)
5. Jia, X., Caroli, C., Velicky, B.: Ultrasound propagation in externally stressed granular media. Phys. Rev. Lett. **82**(9), 1863–1866 (1999)
6. Velea, D., Shields, F.D., Sabatier, J.M.: Elastic wave velocities in partially saturated ottawa sand: experimental results and modeling. Soil Sci. Soc. Am. J. **64**(4), 1226–1234 (2000)
7. Liu, C.H., Nagel, S.R., Schecter, D.A., Coppersmith, S.N., Majmudar, S., Narayan, O., Witten, T.A.: Force fluctuations in bead packs. Science **269**(5223), 513–515 (1995)
8. Mueth, D.M., Jaeger, H.M., Nagel, S.R.: Force distribution in a granular medium. Phys. Rev. E **57**(3), 3164–3169 (1998)
9. Løvoll, G., Måløy, K.J., Flekkøy, E.G.: Force measurements on static granular materials. Phys. Rev. E **60**(5), 5872–5878 (1999)
10. Majmudar, T.S., Behringer, R.P.: Contact force measurements and stress-induced anisotropy in granular materials. Nature **435**(1079), 1079–1082 (2005)
11. Veje, C.T., Howell, D.W., Behringer, R.P.: Kinematics of a two-dimensional granular couette experiment at the transition to shearing. Phys. Rev. E **59**(1), 739–745 (1999)
12. Peters, J.F., Muthuswamy, M., Wibowo, J., Tordesillas, A.: Characterization of force chains in granular material. Phys. Rev. E **72**(4), 041307 (2005)
13. Tordesillas, A., Muthuswamy, M.: On the modeling of confined buckling of force chains. J. Mech. Phys. Solids **57**(4), 706–727 (2009)
14. Albert, I., Tegzes, P., Kahng, B., Albert, R., Sample, J.G., Pfeifer, M., Barabási, A.L., Vicsek, T., Schiffer, P.: Jamming and fluctuations in granular drag. Phys. Rev. Lett. **84**(22), 5122–5125 (2000)
15. Geng, J., Behringer, R.P.: Slow drag in two-dimensional granular media. Phys. Rev. E **71**(1), 011302 (2005)
16. Métayer, J.F., Suntrup III, D.J., Radin, C., Swinney, H.L., Schröter, M.: Shearing of frictional sphere packings. Europhys. Lett. **93**(6), 64003 (2011)
17. Hutchings, I.M.: Energy absorbed by elastic waves during plastic impact. J. Phys. D Appl. Phys. **12**(11), 1819 (1979)
18. McLaskey, G.C., Glaser, S.D.: Micromechanics of asperity rupture during laboratory stick slip experiments. Geophys. Res. Lett. **38**(12), L12302 (2011)
19. Gilardi, G., Sharf, I.: Literature survey of contact dynamics modelling. Mech. Mach. Theory **37**(10), 1213–1239 (2002)
20. Bardenhagen, S.G., Brackbill, J.U.: Dynamic stress bridging in granular material. J. Appl. Phys. **83**(11), 5732–5740 (1998)
21. Owens, E.T., Daniels, K.E.: Sound propagation and force chains in granular materials. Europhys. Lett. **94**(5), 54005 (2011)
22. Cody, G.D., Goldfarb, D.J., Storch, G.V., Norris, A.N.: Particle granular temperature in gas fluidized beds. Powder Technol. **87**(3), 211–232 (1996)
23. Gardel, E., Seitaridou, E., Facto, K., Keene, E., Hattam, K., Easwar, N., Menon, N.: Dynamical fluctuations in dense granular flows. Philos. Trans. R. Soc. A **367**(1909), 5109–5121 (2009)
24. Michlmayr, G., Or, D., Cohen, D.: Fiber bundle models for stress release and energy bursts during granular shearing. Phys. Rev. E **86**, 06130 (2012)
25. Michlmayr, G., Cohen, D., Or, D.: Shear induced force fluctuations and acoustic emissions in granular material. J. Geophys. Res. **118**(12), 6086–6098 (2013)
26. Hidalgo, R.C., Grosse, C.U., Kun, F., Reinhardt, H.W., Herrmann, H.J.: Evolution of percolating force chains in compressed granular media. Phys. Rev. Lett. **89**(20), 205501 (2002)
27. Turcotte, D.L., Newman, W.I., Shcherbakov, R.: Micro and macroscopic models of rock fracture. Geophys. J. Int. **152**(3), 718–728 (2003)
28. Hertz, H.: Über die Berührung fester elastischer Körper (On the contact of elastic solids). Journal für die reine und angewandte Mathematik **92**, 156–171 (1882). For English translation see Miscellaneous papers by Hertz, H. (eds). Jones and Schott. Macmillian, London (1896)
29. Landau, L.D., Lifshitz, E.M.: Theory of Elasticity, 3rd edn. Pergamon Press, Oxford (1986)
30. Bracewell, R.N.: The Fourier Transform and Its Applications, 2nd edn. McGraw-Hill, New York (1986)
31. Hunter, S.: Energy absorbed by elastic waves during impact. J. Mech. Phys. Solids **5**(3), 162–171 (1957)
32. Thornton, C.: Numerical simulations of deviatoric shear deformation of granular media. Geotechnique **50**(1), 43–53 (2000)
33. Mair, K., Hazzard, J.F.: Nature of stress accommodation in sheared granular material: insights from 3d numerical modeling. Earth Planet Sci. Lett. **259**(3–4), 469–485 (2007)
34. Welker, P., McNamara, S.: Precursors of failure and weakening in a biaxial test. Granul. Matter **13**, 93–105 (2011)
35. Pohlman, N.A., Severson, B.L., Ottino, J.M., Lueptow, R.M.: Surface roughness effects in granular matter: influence on angle of

repose and the absence of segregation. Phys. Rev. E **73**(3), 031304 (2006)
36. Zaitsev, S.I.: Robin Hood as self-organized criticality. Physica A Stat. Mech. Appl. **189**(3–4), 411–416 (1992)
37. Buldyrev, S.V., Ferrante, J., Zypman, F.R.: Dry friction avalanches: experiment and theory. Phys. Rev. E **74**(6), 066110 (2006)
38. Sammonds, P., Ohnaka, M.: Evolution of microseismicity during frictional sliding. Geophys. Res. Lett. **25**(5), 699–702 (1998)
39. Yabe, Y.: Rate dependence of AE activity during frictional sliding. Geophys. Res. Lett. **29**(10), 1388 (2002)
40. Mair, K., Marone, C., Young, R.P.: Rate dependence of acoustic emissions generated during shear of simulated fault gouge. Bull. Seismol. Soc. Am. **97**(6), 1841–1849 (2007)
41. Tordesillas, A., Walker, D.M., Lin, Q.: Force cycles and force chains. Phys. Rev. E **81**(1), 011302 (2010)
42. Somfai, E., Roux, J.N., Snoeijer, J.H., van Hecke, M., van Saarloos, W.: Elastic wave propagation in confined granular systems. Phys. Rev. E **72**(2), 021301 (2005)
43. Schmitz, T.L., Smith, K.S.: Mechanical Vibrations: Modeling and Measurement. Springer, New York (2012)
44. Tordesillas, A.: Force chain buckling, unjamming transitions and shear banding in dense granular assemblies. Philos. Mag. **87**(32), 4987–5016 (2007)
45. Radjai, F., Richefeu, V.: Contact dynamics as a nonsmooth discrete element method. Mech. Mater. **41**(6), 715–728 (2009)
46. Raischel, F., Kun, F., Hidalgo, R.C., Herrmann, H.J.: Statistical Damage Models: Fiber Bundle Models, chapter Statistical Damage Models: Fiber Bundle Models, pp. 443–471. Universität Stuttgart (2006)
47. Dalton, F., Petri, A., Pontuale, G.: A random neighbour model for yielding. J. Stat. Mech. Theory Exp. **2010**(3), P03011 (2010)
48. Pradhan, S., Hemmer, P.C.: Prediction of the collapse point of overloaded materials by monitoring energy emissions. Phys. Rev. E **83**(4), 041116 (2011)
49. Peires, F.T.: Tensile tests for cotton yarns V. The weakest link: theorems on the strength of long composite specimens. J. Text. Inst. **17**, T355–T368 (1926)
50. Daniels, H.E.: The statistical theory of the strength of bundles of threads. 1. Proc. R. Soc. A **183**(995), 405–435 (1945)
51. Timár, G., Kun, F.: Crackling noise in three-point bending of heterogeneous materials. Phys. Rev. E **83**(4), 046115 (2011)
52. Raischel, F., Kun, F., Herrmann, H.J.: Simple beam model for the shear failure of interfaces. Phys. Rev. E **72**(4), 046126 (2005)
53. Halász, Z., Kun, F.: Slip avalanches in a fiber bundle model. Europhys. Lett. **89**(2), 26008 (2010)
54. Halasz, Z., Kun, F.: Fiber bundle model with stick-slip dynamics. Phys. Rev. E **80**(2), 027102 (2009)
55. Kruyt, N.P., Antony, S.J.: Force, relative-displacement, and work networks in granular materials subjected to quasistatic deformation. Phys. Rev. E **75**(5), 051308 (2007)
56. Skempton, A., Bishop, A.: The measurement of the shear strength of soils. Geotechnique **2**(2), 98–108 (1950)
57. Thornton, C., Zhang, L.: Numerical simulations of the direct shear test. Chem. Eng. Technol. **26**(2), 153–156 (2003)
58. Cui, L., O'Sullivan, C.: Exploring the macro- and micro-scale response of an idealised granular material in the direct shear apparatus. Geotechnique **56**(7), 455–468 (2006)
59. Liu, S.H.: Simulating a direct shear box test by dem. Can. Geotech. J. **43**(2), 155–168 (2006)
60. Kozicki, J., Niedostatkiewicz, M., Tejchman, J., Muhlhaus, H.B.: Discrete modelling results of a direct shear test for granular materials versus FE results. Granul. Matter **15**(5), 607–627 (2013)